Available online at www.sciencedirect.com
SCIENCE DIRECT®
Journal of Chromatography A, 1013 (2003) 77–91
JOURNAL OF CHROMATOGRAPHY A
www.elsevier.com/locate/chroma

Diffusion coefficient measurement in a microfluidic analyzer using dual-beam microscale-refractive index gradient detection Application to on-chip molecular size determination

Colin D. Costin, Roy K. Olund, Bethany A. Staggemeier, Ana Kristine Torgerson, Robert E. Synovec*

Center for Process Analytical Chemistry (CPAC), Department of Chemistry, Box 351700, University of Washington, Seattle, WA 98195-1700, USA

Abstract

We report a microchip-based detection scheme to determine the diffusion coefficient and molecular mass (to the extent correlated to molecular size) of analytes of interest. The device works by simultaneously measuring the refractive index gradient (RIG) between adjacent laminar flows at two different positions along a microchannel. The device, referred to as a microscale molecular mass sensor (μ-MMS), takes advantage of laminar flow conditions where the mixing of two streams occurs essentially by diffusion across the boundary between the two streams. Two flows merge on the microchip, one containing solvent only, referred to as the mobile phase stream and one which contains the analyte(s) of interest in the solvent, i.e. the sample stream. As these two streams merge and flow parallel to each other down the microchannel a RIG is created by the concentration gradient. The RIG is further influenced by analyte diffusion from the sample stream into the mobile phase stream. Measuring the RIG at a position close to the merging point (upstream signal) and simultaneously a selected distance further down the microchannel (downstream signal) provides real-time data related to the extent a given analyte has diffused, which can be readily correlated to analyte molecular mass by taking the ratio of the downstream-to-upstream signals. For the dual-beam RIG measurements, a diode laser output is coupled to a single mode fiber optic splitter with two output fibers. Light from each fiber passes through a graded refractive index (GRIN) lens forming a collimated beam that then passes through the microchannel and then on to a position sensitive detector (PSD). The RIG at both detection positions deflects the two collimated probe beams. The deflection angle of each beam is then measured on two separate PSDs. The μ-MMS was evaluated using polyethylene glycols (PEGs), sugars, and as a detector for size-exclusion chromatography (SEC). Peak purity can be readily identified using the μ-MMS with SEC. The limit of detection was 0.9 ppm (PEG at 11 840 g/mol) at the upstream detection position corresponding to a RI limit of detection (LOD) (3σ) of $7 \cdot 10^{-8}$ RI. The pathlength for the RIG measurement was 200 μm and the angular LOD was 0.23 μrad with a detection volume of 8 nl at both positions. The average molecular mass resolution was 9% (relative standard deviation) for a series of PEGs ranging in molecular mass from 106 to 22 800 g/mol. With this excellent mass resolution, small molecules such as monosaccharides, disaccharides, and so on, are readily distinguished. The sensor is demonstrated to readily determine unknown diffusion coefficients.

Keywords: Diffusion coefficients; Microfluidics; Chip technology; Refractive index gradient detection; Detection, LC; Poly(ethylene glycol)

*Corresponding author. Tel.: +1-206-685-2328; fax: +1-206-685-8665.
E-mail address: synovec@chem.washington.edu (R.E. Synovec).

0021-9673/03/$ – see front matter
doi:10.1016/S0021-9673(03)01101-4

1. Introduction

The ongoing development of micro-total analysis systems (μ-TAS) have given us new and exciting analytical devices and have pushed forward many of the technical barriers that keep micro-instrumentation from achieving wider use. While μ-TAS can often provide fast, accurate, and low cost analyses, one of the biggest hurdles for μ-TAS gaining greater applicability has been the lack of sensitive and informative universal detection techniques [1,2]. Here we report a novel universal detection technique that gives near real-time information for analyte diffusion coefficient, molecular mass and concentration in a microfabricated device using pressure driven flow. The ability to rapidly make diffusion coefficient measurements within a microfabricated device is an important capability for capillary and microchannel electrophoresis applications [3].

Previously, we reported a microchip detection scheme, the micro-scale refractive index gradient (μ-RIG) detector, that monitored the concentration gradient created between two merging laminar streams flowing within a microchannel and demonstrated universal detection for microfluidic devices [4]. One of the streams contained the analyte of interest in a solvent, called the sample stream, and the other stream contained the solvent only, called the mobile phase stream. The μ-RIG detector was shown to be a simple, compact, low cost refractive index (RI) detector. In the work reported herein, it will be demonstrated that the μ-RIG detector performs at, or better than, the limit of detection reported for other microscale RI detectors [5–7], while providing additional analyte information [8]. In that previous report [8], the μ-RIG detector was demonstrated to provide molecular size information, i.e. molecular diffusion and molecular mass. Here we refer to it in a dual-beam mode as a micro-scale molecular mass sensor (μ-MMS) [8]. The μ-MMS applies the same principles as the μ-RIG detector, but the concentration gradient is probed at two different positions along a microchannel: the upstream detection position is close to the merging point of the two streams and the downstream detection position is further down the microchannel. The distance between the two positions gives time for analyte to diffuse, which decreases the concentration gradient and thus the RIG according to the analyte diffusion coefficient, providing a correlation to molecular mass for a given class of compounds.

This initial report [8] provided proof-of-principle methodology to determine diffusion coefficients and molecular mass using a microchip with pressure driven flow. However, the initial μ-MMS was a single-beam device, thus for a given set of analytes, all the samples were first run and detected at the upstream detection position. The instrument was then realigned to probe the downstream detection position and the set of samples were run again. Finally, the upstream and downstream data sets were evaluated to ascertain the diffusion coefficient and molecular mass information. This was a rather tedious process and introduced a significant level of experimental noise and error. The dual-beam μ-MMS reported herein provides a significant improvement with the upstream and downstream detection positions now probed simultaneously using two different probe beams from a single diode laser source, and two different position sensitive detectors (PSDs) for the detection of the deflected probe beams.

Refractive index detection for high performance liquid chromatography (HPLC) and capillary electrophoresis (CE) has been a reliable universal detection technique for many years [9–19], especially for analytes that do not naturally lend themselves to absorbance or fluorescence detection. There are examples of RI detectors that probed the axial RIG [14–16] at a single detection position and also a detector that probed the radial RIG to make molecular mass measurements [20,21]. Building on this work, the μ-MMS has the potential to serve both as a sensitive, universal μ-TAS detector and as a detector for bench-top HPLC and CE, providing concentration, peak purity, diffusion coefficient and molecular mass information all from a single run. Indeed, the μ-MMS is based upon applying well-established fundamental principles of detection and microfluidics.

There are a number of reported instances where researchers have taken advantage of laminar flow conditions at low Reynolds number in microfluidic devices to do biochemical analysis. One such property of these devices is that when two streams merge and flow parallel to each other down a common channel the only mixing that occurs is due to diffusion across the boundary between the streams. A device called the T-sensor [22–25] uses this

principle for detecting analytes, however it requires the use of fluorescent probes for detection. Another very similar device known as the H-filter [26] also takes advantage of the diffusive mixing properties of laminar flows to separate analytes by size and has been used to do sample preparation for HPLC [27]. With the μ-MMS, we describe a means of universally detecting the concentration gradient that is created between the two streams as analyte diffuses from a sample stream into a mobile phase stream (Fig. 1). This is done by measuring the deflection of a laser probe beam, incident on a microchannel, orthogonal to both the direction of flow and the concentration gradient, by the RIG generated by the transverse diffusion of analyte from the sample stream into the mobile phase stream.

With the μ-MMS the upstream and downstream detection positions are probed simultaneously using two different probe beams from a single diode laser source, and two different position sensitive detectors (PSDs) for the detection of each of the deflected probe beams. The downstream signal divided by the upstream signal (ratio signal) correlates to analyte diffusion coefficient and molecular mass and is obtained in near real-time. The new dual-beam system is evaluated by flow injection analysis (FIA) of polyethylene(glycol)s and sugars, and is also demonstrated as a detector for size-exclusion chromatography (SEC). The individual upstream and downstream signals, along with the ratio signal, all as a function of time during the FIA and chromatographic experiments, provide concentration, diffusion coefficient and molecular mass information for a given sample. Furthermore, peak purity can be ascertained using the ratio signal as a function of time from the SEC data. The limit of detection is evaluated, as is the concentration dependence of the ratio signal. It is critical that the ratio be independent of analyte concentration in order to readily allow correlation of the ratio signal to diffusion coefficient and molecular mass. The molecular mass resolution is also evaluated using the PEGs and sugars. The potential to make diffusion coefficient measurements on-chip is also demonstrated.

2. Theory

Microfluidic systems are generally operated at very low Reynolds number conditions, thus the flows exhibit laminar properties. When two streams merge on a microchip under laminar flow conditions the streams will not undergo turbulent mixing, instead they mix by diffusion across a distinct boundary between the streams. A simple approach to discussing this system is to use the one-dimensional diffusion equation known as Fick's law, although a two-dimensional approach would be more rigorous [28,29]:

$$\frac{dC}{dt} = \frac{d}{dx}\left(D \cdot \frac{dC}{dx}\right) \quad (1)$$

where C is analyte concentration, D is the analyte diffusion coefficient, and x is the direction of analyte migration. Eq. (1) describes the time-dependent concentration gradient of a given analyte as a function of its diffusion coefficient. There have been a number of studies attempting to model this behavior and researchers have determined that diffusion does not occur strictly according to Eq. (1) [23,29] since diffusion is actually occurring in two dimensions. While this may be important for certain applications, diffusion in the second dimension can be neglected for the sake of simplicity in the discussion of the detection mechanism with the μ-MMS. Here, we are primarily concerned with diffusion occurring orthogonal to the direction of flow and orthogonal to both probe beams. Also, the flow direction and the two, parallel probe beams are orthogonal to each other (see Fig. 1).

Pawliszyn [15] has previously described the measurement of the deflection angle of a non-absorbed probe beam on a position sensitive detector that occurs due to presence of an analyte concentration gradient, and thus, a refractive index gradient:

$$\theta = \frac{L}{n_0} \cdot \frac{dn}{dx} = \frac{L}{n_0} \cdot \frac{dn}{dC} \cdot \frac{dC}{dx} \quad (2)$$

where θ is the angle of deflection, L is the path length the laser probe beam takes through the flow cell orthogonal to the RIG, n_0 is the refractive index of the solvent and dn/dx is the analyte RIG influenced by diffusion. As the analyte from the sample stream merges with an adjacent mobile phase stream a concentration gradient is formed, which creates the RIG. The RIG will deflect a laser probe beam according to Eq. (2), and in the absence of a

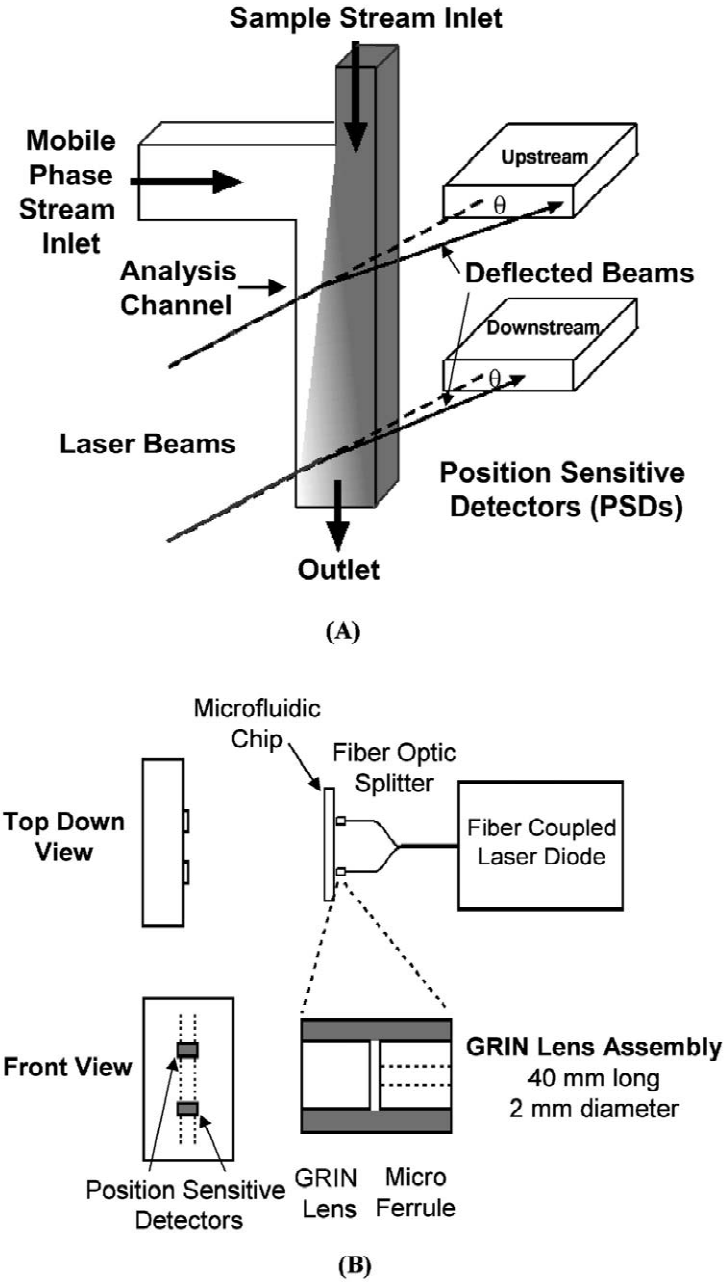

Fig. 1. Illustration of the dual-beam microscale-molecular mass sensor (μ-MMS) with the type A chip design shown. (A) A sample stream (dark, for illustration purposes only) merges with a mobile phase stream (light) in the analysis channel. Two parallel, collimated laser beams probe the analyte concentration gradient in the analysis channel at two different positions, upstream (close to the merge point) and downstream. The two probe beams are orthogonal to both the direction of flow and the analyte concentration gradient, and pass through the channel and impinge on two position sensitive detectors (PSDs). As analyte enters the analysis channel, creating a concentration gradient, the beams are deflected from their default positions (dotted lines). The angle of deflection is detected by each PSD. (B) A laser diode is coupled to a fiber optic splitter and the two output beams are collimated by two GRIN lens assemblies. The two beams pass through the microchannel and continue onto the two PSDs.

RIG no deflection would be observed. The magnitude of the RIG is diminished by analyte diffusion according to Eq. (1), from the sample stream to the mobile phase stream. The dual beam μ-MMS measures the extent of diffusion by probing the RIG at two positions separated in distance down the channel, and thus, the time difference for diffusion to occur.

The RIG signal is measured at the upstream and downstream detection positions, in Fig. 1. Utilizing the impact that Eq. (1) has on the angle measurement determined by Eq. (2), and taking the ratio, R, of the signals (Eq. (3)) one can empirically distinguish the difference in diffusion coefficient between one analyte and another:

$$R = \frac{\theta(t)\text{Downstream}}{\theta(t)\text{Upstream}}, \quad 0 \leq R \leq 1 \tag{3}$$

where $\theta(t)$ represents the signal as a function of time for the position being probed. One can rationalize Eq. (3) by thinking about how Eqs. (1) and (2) are related. Eq. (1) describes the time dependent change in concentration as an analyte with a given diffusion coefficient diffuses over some distance (with diffusion orthogonal to both the direction of flow and to the direction of a given probe beam). Eq. (2) then describes a set of conditions used to measure the resulting RIG created as a given analyte diffuses as a function of time and distance. Measuring the concentration gradient at two positions along the same flow axis, some distance apart, is equivalent to measuring the concentration gradient of a diffusing analyte at two different times. Thus taking the ratio of the downstream to upstream signals via Eq. (3) allows other variables in Eqs. (1) and (2) to cancel, providing a means to directly correlate sensor data to diffusion coefficient and, for a particular class of compounds, to molecular mass.

3. Experimental

3.1. System construction

The design of the μ-MMS is shown in Fig. 1 and is similar to a previously reported design [8] but with several notable differences. A variable power fiber coupled 635 nm single mode diode laser (Thor Labs, S1FC635, Newton, NJ, USA) is connected to a 1×2 single mode fiber optic coupler with an FC connector at the input and bare fibers for both beam outputs (Newport, F-CPL-1x2-OPT-50-10-NN, Irvine, CA, USA). The two bare fiber outputs are then affixed to 0.25 pitch, 1.0 mm GRIN lenses (Newport, LGI630-2). Each GRIN lens assembly is then mounted on to individual 3D translational stages (Melles Griot, MicroLab Translational Stages, Irvine, CA, USA) allowing each GRIN lens assembly to be moved independently for easy alignment of the laser probe beams upon the microchannel as indicated in Fig. 1. The two probe beams were then aligned on an in-house made poly(dimethyl siloxane) (PDMS) microchannel, which was mounted on a high precision x–y–z translational stage (Newport, 460-x-y-z, Fountain Valley, CA, USA) to allow the microchip to be moved within the probe beams. The two probe beams passed through the PDMS microchannel and were each detected on two separate one-dimensional PSDs (Hamamatsu, S3932, Hamamatsu, Japan), which were mounted on an in-house made circuit box which allowed them to be moved relative to each other in order to change the separation distance between the detection zones. The PSDs were mounted on a high precision x–y–z translational stage (Newport, 460-x-y-z, Fountain Valley, CA, USA), such that the long axes of both PSDs were oriented orthogonal to the microchannel, at a distance of 90 cm from the microchannel. The distance between the microchannel and detection plane was limited by the probe beam divergence relative to the PSD width. The deflections of each diode laser beam were then monitored by the long axis of each PSD and read into a personal computer by a data acquisition board (DAQ) (National Instruments, SCB-68, Austin, TX, USA). Data acquisition and instrument control software was written in house with LabVIEW software (National Instruments, LabVIEW student version 6i, Austin, TX, USA). The diode laser probe beam system, microchannel structure, and PSDs were all mounted on a standard 5×2 ft optical breadboard (Newport, Fountain View, CA, USA) with a foam base and were enclosed in a housing (made in-house) to minimize noise due to vibration, stray light, and temperature fluctuations.

3.2. Microchannel design, fluid control and detection optimization

Two different microchannel designs were explored, type A and type B. The channel dimensions and configuration were different between the two designs, and will be pointed out appropriately throughout the text. Fig. 1A shows a schematic of the type A design where the sample and mobile phase inlet channels merge 90° relative to each other and flow through an analysis channel. The microchannel network for the type A design was relatively simple consisting of a smaller channel, introducing sample into the analysis channel and a larger channel, introducing mobile phase into the analysis channel. Both the analysis channel and mobile phase inlet dimensions were 500 μm wide × 200 μm deep, for the type A design, with the analysis channel 3.5 cm long and the mobile phase inlet 2 cm long. The sample inlet channel dimensions for the type A design were 100 μm wide × 200 deep μm deep × 1 cm long. The type B design, not shown for brevity, had the sample and mobile phase inlet channels merge 180° relative to each other, and then flow through the analysis channel making the type B design similar to the previously reported T-sensor [24]. The type B design had the same dimensions for the analysis channel except the length of the channel was increased to 5.6 cm. The sample inlet and mobile phase inlet channels were 100 × 200 μm × 1 cm for the type B design. The microfluidic chips used in all experiments reported herein were made using well-documented soft lithography techniques [30–32]. Interconnects to the type A and B micro channels were made using 10 cm segments of 1/16 inch O.D. polyether ether ketone (PEEK) tubing (1 in. = 2.54 cm), with the I.D. of the tubing 63.5 μm for the sample inlet, 127 μm for the mobile phase inlet, and 254 μm for the outlet (Upchurch Scientific, Oak Harbor, WA, USA). The segments were then sealed to the channel using an epoxy, H74F (Epoxy Technology Inc, Billerica, MA). The microchips were integrated into the rest of the instrumentation by fitting the opposite ends of PEEK tubing with Superflangeless HPLC fittings (Upchurch Scientific). Fluid was pumped through the μ-MMS chip using two syringe pumps (Isco, μLC 500, Lincoln, NE, USA). One syringe pump was used for the sample stream and the other pump used for mobile phase. The sample stream passed through an eight-port auto-injection valve (Rheodyne, LabPRO, Rohnert Park, CA, USA). The sample stream composition was equivalent to the mobile phase stream (i.e. solvent) except for when a sample was injected. The sample injection into the sample stream and onto the microchip was controlled through a DAQ board, again using LabVIEW software. Note that in contrast to our previous report [8], no split was applied to the sample stream with the experiments reported herein.

The system was configured as shown in Fig. 1 so both probe beams would be incident upon the analysis channel orthogonal to both the direction of flow and the concentration gradient at two detection positions, upstream and downstream, along the axis of flow. Both the upstream and downstream-detected angle data were collected after aligning both incident diode laser beam positions to provide optimum sensitivity. The optimum detection positions were determined for both the upstream and downstream detection positions using a 5‰ (w/v) solution of 22 800 g/mol PEG using a method we previously reported [4]. The upstream detection position was approximately 500 μm past the initial merging point of the sample and mobile phase streams and the downstream detection position was located 2.7 cm beyond the upstream detection position for both type A and type B chips. All data from the two PSDs were analyzed using ORIGIN software (Microcal Software, Northampton, MA, USA) and MATLAB software (Mathworks, Natick, MA, USA).

3.3. Polymer and sugar experiments

PEG and sugar solutions were used to evaluate the performance of the sensor. In all of the flow injection analysis (FIA) experiments, when using a 20-μl injected volume, it was experimentally determined that the sample entering the sensor was at the injected concentration at the detected peak maximum (not diluted at peak maximum). PEG standards (Polymer Labs., Amherst, MA, USA) were studied and are listed in Table 1 with their polydispersity values and diffusion coefficients calculated by Eq. (4) [21]:

Table 1
PEG standards with their average molecular mass (in g/mol), polydispersity, and diffusion coefficient

Poly(ethylene glycol) samples	Average molecular mass (g/mol)	Polydispersity	Diffusion coefficient D ($\times 10^{-7}$ cm^2/s)
PEG 106	106	1.00	96.2
PEG 194	194	1.00	69.0
PEG 400	400	1.05	46.3
PEG 620	620	1.05	36.4
PEG 1080	1080	1.04	26.8
PEG 1900	1900	1.03	19.7
PEG 4120	4120	1.02	12.8
PEG 6450	6450	1.02	10.0
PEG 11 840	11 840	1.04	7.19
PEG 22 800	22 800	1.06	5.01

$$D_{\mathrm{PEG}} = 1.25 \cdot 10^{-4}(\mathrm{MM})^{-0.55} \quad (4)$$

where D is the calculated diffusion coefficient, assuming a random coil configuration, and MM is the average molecular mass of the polymer in g/mol. The sugar samples (all from Sigma-Aldrich, St. Louis, MO, USA) were studied without further purification. The FIA experiments were repeated five times for each solution unless specified otherwise. PSD data were collected at both the upstream and downstream detection positions simultaneously for each run. The data shown in Figs. 2, 3, 5, and 6 were run using the type A chip design, which required flow rate balancing such that the sample inlet flow did not occupy the majority of the analysis channel volume at the merge point. Since the sample and mobile phase inlet channels had different cross-sectional areas for the type A chip design, the volumetric flow rates had to be tuned such that the channel volume occupied by each flow at the merging point was approximately equal. The data shown in Figs. 4 and 7 were collected using the type B design and were repeated three times. No significant performance differences were observed using the two chip designs.

3.4. Chromatography experiments

The size-exclusion chromatography experiments were run on a 250×2.1 mm SynChropak HPLC column with a GPC 100 stationary phase (EIChrom, Darien, IL, USA), using a 5-μl injection volume. The SEC experiments were performed using a type B chip in the μ-MMS. Since the type B chip design had sample and mobile phase inlet channels of the same dimension, both flows were set at the same volumetric flow rate of 20 μl/min. The column was inserted in to the instrument between the injection valve and the microchip. A two-component mixture was evaluated consisting of PEGs 22 800 and 106 at an injected concentration of 2‰ each. The separation for each mixture was run in triplicate to ascertain reproducibility.

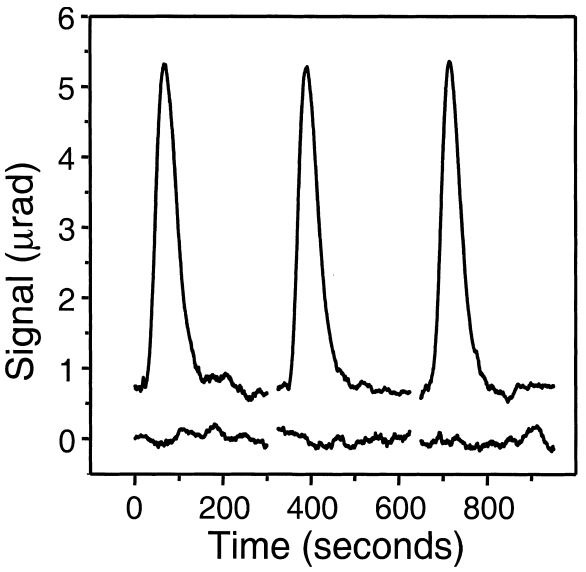

Fig. 2. Three repeated 20-μl injections of 20 ppm aqueous PEG 11 840 with representative sections of baseline are shown, using a mobile phase at 20 μl/min and sample flow rate at 10 μl/min and the type A chip design. The limit of detection was calculated to be 0.9 ppm using 3σ statistics. PEG signal traces are offset by 0.75 μrad for clarity.

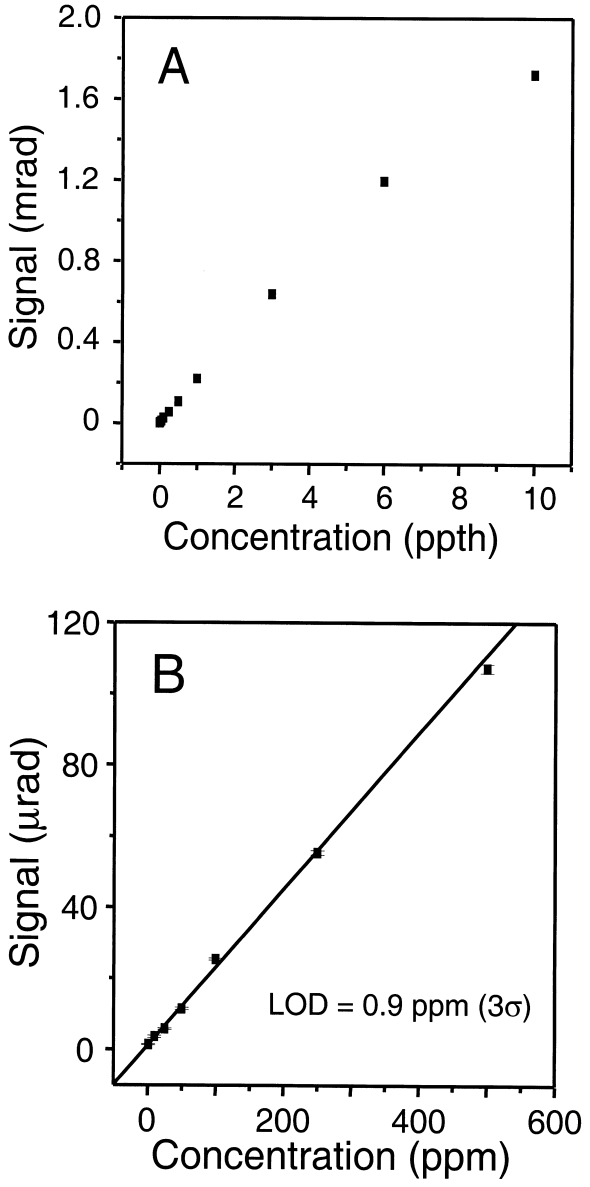

Fig. 3. (A) Calibration plot of signal versus concentration (w/v) for aqueous solutions of PEG 11 840 reported as maximum peak height (deflection angle) taken at the upstream detection position using same conditions as in Fig. 2. Each point represents the average of three repeated 20-μl injections, with the error bars too small to be observed on this scale. (B) Expanded view showing the linearity at lower concentrations, from 1 to 500 ppm. The slope of the best-fit line is 219.46 μrad/ppm with an intercept of −1.13 μrad and a correlation coefficient of 0.9977.

4. Results and discussion

The performance of the improved μ-RIG detector was evaluated. Typical signal and baseline traces from the upstream detection position are shown in Fig. 2 for a 20 ppm PEG 11 840 solution. Using the baseline and PEG 11 840 data, the limit of detection (LOD) was investigated using 3σ statistics. The LOD of the detected angle of beam deflection was determined to be 0.23 μrad with a standard deviation of±0.02 μrad. Using the data in Fig. 2, the concentration LOD for PEG 11 840 was found to be 0.9 ppm, with a standard deviation of ±0.1 ppm. From this information and a measured dn/dC for PEG 11 840 of $8\cdot10^{-8}$ RI/ppm the effective refractive index LOD is $7\cdot10^{-8}$ RI. These new LOD values are a significant improvement over the previously reported LODs [8] of 1.43 μrad, 56 ppm, and $4.5\cdot10^{-6}$ RI using the same analyte and detection mechanism. This improvement is due to several advances in the design of the sensor. The depth of the microchannel was increased from 30 to 200 μm, which according to Eq. (2) should improve the LOD about 7-fold. Another change leading to the improvement in the LOD was the use of a GRIN lens to collimate each diode laser probe beam over a longer distance, leading to an amplification of the deflection distance for a given deflection angle. Also, the dual-beam instrument used a different PSD model, which had a significantly larger position displacement resolution, again producing roughly a 7-fold improvement. All of the improvements together account for the ~60-fold improvement in the concentration LOD achieved compared to our previous report.

In order to be useful for a variety of applications, the μ-RIG detector should have a large linear dynamic range. Evaluation of dynamic range was performed using aqueous solutions of PEG 11 840 run at different concentrations. The resulting calibration plots are shown in Fig. 3. The solutions were made from the serial dilution of a 10‰ stock solution, ranging in concentration from 1 ppm to 10‰. Fig. 3A shows the average of three 20 μl injections at each concentration. The error bars in the measurements (±1 standard deviation) were too small to be seen in the plot. Fig. 3B shows an expanded view of the same calibration plot for the more dilute solutions from 1 to 500 ppm. The data

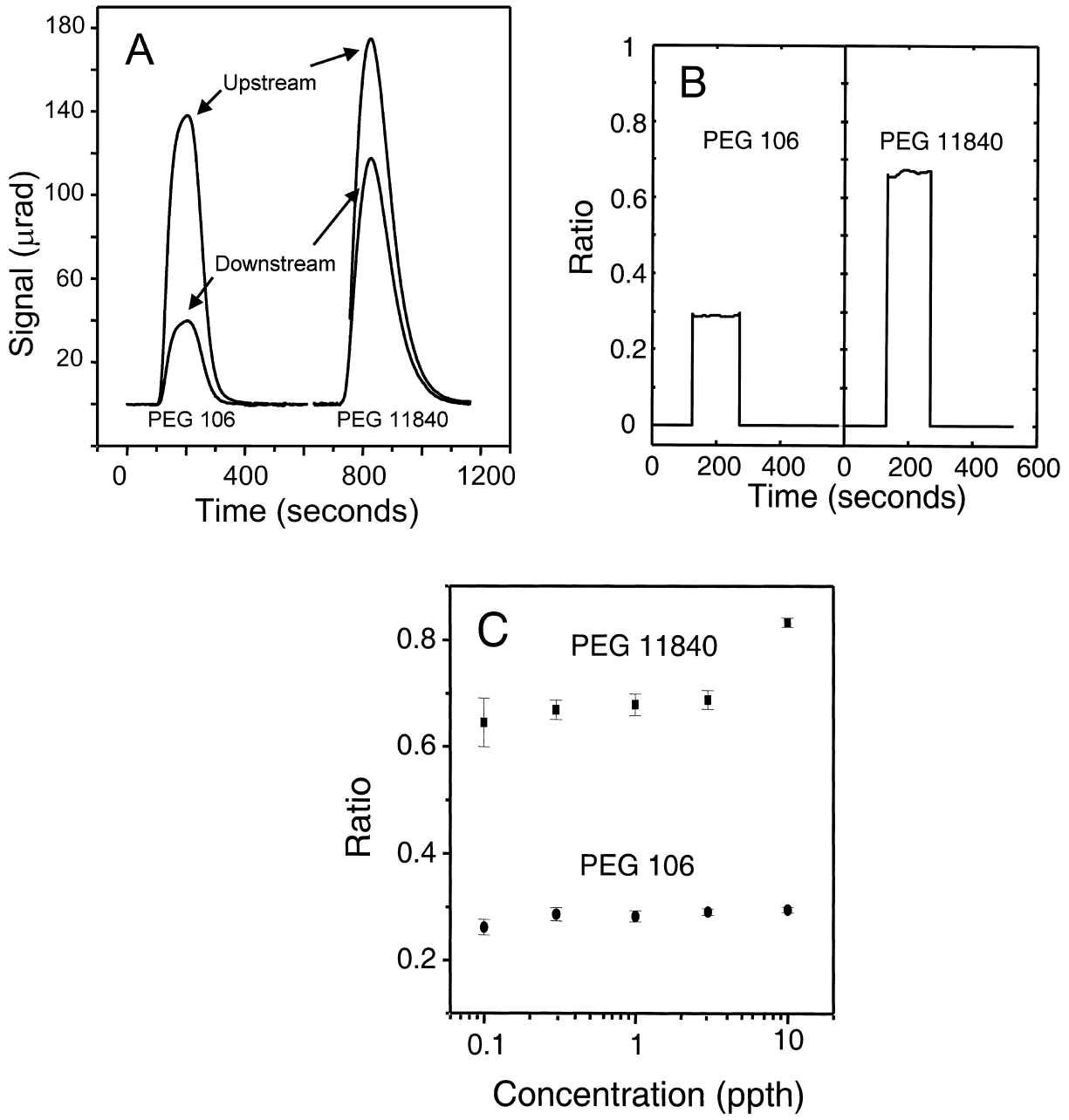

Fig. 4. (A) Signal versus time for aqueous solutions of PEG 106 and PEG 11 840 simultaneously collected with the μ-MMS at the upstream and downstream detection positions. The data was collected using the type B channel design with a flow rate of 10 μl/min in both the mobile phase and sample streams, with the data corrected for the 7-s time delay between the two detection positions. Injection volume was 20 μl at a concentration of 1‰. (B) Ratio, *R* (downstream signal divided by the upstream signal), in (A) as a function of time, i.e. the ratiogram, for PEG 106 and PEG 11 840. (C) Ratio versus concentration for aqueous solutions of PEG 106 and PEG 11 840 made by serial dilution of a 10‰ (w/v) stock solution. Each point represents the average of three 5-μl injections of each solution, with errors bars shown as one standard deviation.

demonstrate a very good linear fit over this concentration range. It can be seen on Fig. 3A that there is a slight deviation in linearity for the two highest concentration samples. This is likely due to a well-documented [24] characteristic of microfluidics where the volume occupied by each stream (mobile phase and sample), when adjacent streams run parallel down a microchannel, is proportional to the flow rate and the viscosity of each stream. At the higher concentrations the viscosity of the sample stream may increase relative to the mobile phase stream enough to change the spatial position of the RIG, thus causing a deviation from linearity in the calibration curve. In practice, the analyst should strive to work in the linear range or be willing to accept some non-linearity in the calibration.

The current characterization of the μ-RIG detector has so far demonstrated the potential of the device as a reliable, sensitive, and universal single channel detector. Now in the dual-beam mode as a μ-MMS, we will focus on the added ability to measure the analyte diffusion coefficient and correlate this to the analyte molecular mass for a given class of compounds. This is facilitated by measuring the RIG signals for a set of samples from two different detection positions along the analysis channel. Fig. 4A shows an example of the upstream and downstream signals for PEG 11 840 and PEG 106, both injected at the same 1‰ concentration. This figure represents a measurement of the diffusion that has occurred between the upstream and downstream positions for a sample consisting of a small molecule (PEG 106) and a large molecule (PEG 11 840). Since the PEG 106 is so much smaller than the PEG 11 840 it will diffuse across the microchannel more quickly leading to a proportionately more diffuse concentration gradient at the downstream position, which results in a smaller RIG signal. A convenient way to look at the data collected with the μ-MMS is to plot the ratio of the downstream and upstream signals as a function time, as defined in Eq. (3) and shown in Fig. 4B, which is referred to as a ratiogram. Here a more quantitative presentation of the data shows that by looking at the ratio of the two signals one can differentiate molecular mass. It should be noted that when making a ratiogram a threshold value is set at which all data less than the threshold are set to a default ratio of zero. In the case of Fig. 4B this threshold was 10 μrad in Fig. 4A. A larger, more slowly diffusing analyte such as PEG 11 840 yields a larger ratio signal as the analyte has diffused less over the distance between the detection zones. Whereas, a smaller, more quickly diffusing analyte such as PEG 106 yields a much smaller ratio signal as it has had ample time to diffuse. An additional analytical feature of interest in the ratiogram is the degree of flatness for the ratio values. In the FIA experiments used for Fig. 4, the ratio values are naturally flat. However, as we shall see, for size-exclusion chromatography or other forms of HPLC, the flatness or lack thereof of the ratio will provide information regarding polydispersity or peak purity.

Another important aspect of ascertaining the utility of the μ-MMS is to see that the ratio signals are indeed a result of analyte diffusion coefficient differences and not due to a concentration dependent effect. In order to evaluate this issue a series of solutions of varying concentration were prepared from a 10‰ stock solution for both PEG 106 and PEG 11 840. The resulting ratio signals, measured as a function of concentration, are shown in Fig. 4C. If the device is functioning appropriately, one would expect to see different ratios for the two PEGs, but a given PEG should have the same ratio regardless of concentration. Fig. 4C demonstrates this functionality quite well for both PEGs where the different concentrations of a given PEG give a very similar ratio. However, at extremely high concentrations the PEG 11 840 exhibits a deviation to a higher ratio. This deviation is caused by the same viscosity effect that was observed in the calibration plot (Fig. 3A). One can also notice that this effect is not observed for the PEG 106, as expected since the molecular mass is so much smaller and a much larger concentration change is required to significantly effect its viscosity.

A large series of PEGs (Table 1) were studied to determine the diffusion coefficient dependence on the ratio signal. Using the μ-MMS, the peak areas were obtained from the upstream and downstream signals for each PEG, and the areas plotted as a function of PEG diffusion coefficient (Fig. 5A). The data provides insight into the basic mechanism of the sensor. For the upstream peak area data set, one can see that the larger (~greater than 1000 g/mol),

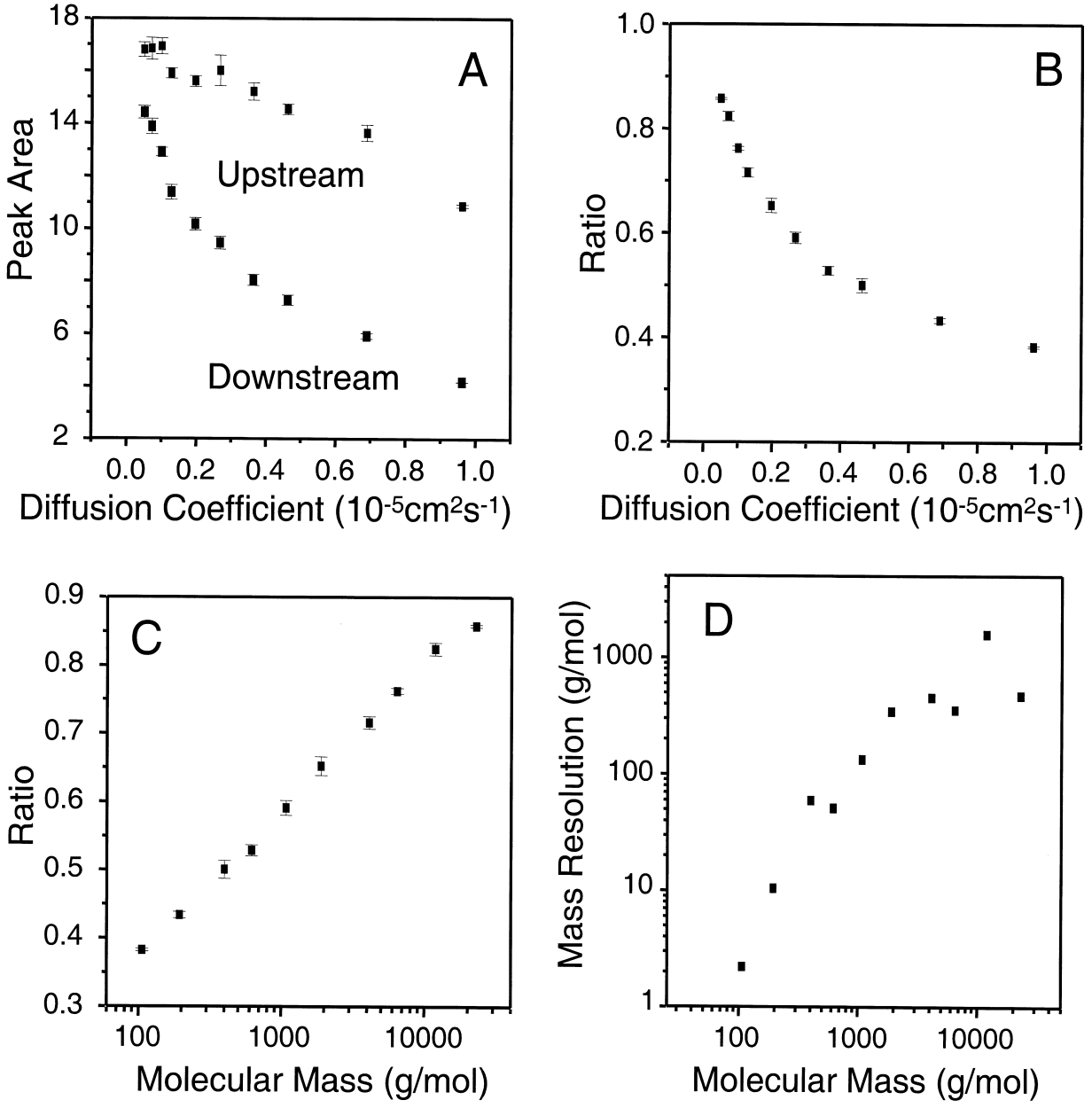

Fig. 5. (A) Peak area (arbitrary units) versus diffusion coefficient taken at the upstream and downstream detection positions for aqueous PEG solutions (see Table 1) at a concentration of 5‰ each, at 20 μl injected. Each point represents an average of five runs with error bars of one standard deviation. A type A channel design was applied with a flow rate of 10 μl/min in the mobile phase stream and 5 μl/min in the sample stream. (B) Ratio, *R*, as a function of diffusion coefficient where the ratio is the downstream/upstream signals from the data plotted on A. (C) Ratio versus molecular mass in g/mol (log scale) for the aqueous PEG solutions. (D) Mass resolution as a function of molecular mass in g/mol (log scale) for the aqueous PEG solutions. Each data point represents the difference between the high and low predicted molecular masses based on the ratio values and±standard deviation error bars shown in C.

slower diffusing PEGs give very similar peak areas, while the smaller PEGs (~less than 1000 g/mol) have had enough time to diffuse to some extent so the peak areas decrease. For the downstream peak area data set, the larger PEGs have now had sufficient time to diffuse, about 10 s, and all PEG peak areas decrease as their diffusion coefficients increase. At the upstream position only the smallest compounds have had time to diffuse and even those have not diffused much, which leads to a relatively sharp concentration gradient for all analytes. At the downstream position ample time has passed to allow many of the smaller analytes to diffuse further across the channel, thus giving a more diffuse concentration gradient for all except the larger PEGs.

The information gleaned from Fig. 5A provides the fundamental picture of how the μ-MMS works. However, it is even more convenient to look at the ratio of the peak areas, which gives a clearer picture of how the samples can be differentiated building from the discussion of Fig. 4. The data shown in Fig. 5B is the ratio of the downstream/upstream data from Fig. 5A plotted for each different PEG as a function of diffusion coefficient. A qualitative extrapolation of the data would indicate that as the diffusion coefficient goes to zero the ratio goes to one, as one would expect. On the other hand, extrapolating the diffusion coefficient to infinity yields a ratio that approaches a minimum value. The ratio data can also be correlated to molecular mass as shown in Fig. 5C. An exceptional correlation is achieved in Fig. 5C where one can readily determine the average molecular mass of an analyte with precision of about 9% of its average molecular mass (relative standard deviation of the molecular mass) shown in Fig. 5D. For example, we can readily distinguish a species with a molecular mass of 100 g/mol from one with a molecular mass of 120 g/mol with a two standard deviation confidence. Thus, a high level of molecular mass selectivity was obtained for the smaller PEGs. This quantifies the average molecular mass resolution for a given PEG and again shows that the system is tuned such that the smaller PEGs will have a lower absolute g/mol resolution than the larger PEGs. The molecular mass resolution is dependent on the flow conditions and chip design for the experiments described here and it is conceivable that the molecular mass range, or diffusion coefficient range, of interest could be readily tuned to look at larger analytes by changing the chip design and/or flow rates.

A series of sugar samples were also studied using the μ-MMS to demonstrate an interesting class of low molecular mass compounds for which the technique can be applied. The ratio signal is plotted as a function of molecular mass in Fig. 6A. Excellent mass resolution is achieved for these small sugars, a result consistent with the smaller PEGs (Fig. 5C and D). Another interesting aspect of the sugar study is that both sucrose and lactose have the same molecular mass but different diffusion coefficients due to slight differences in chemical structure. Plotting the ratio as a function of diffusion coefficient in Fig. 6B, instead of molecular mass, more clearly demonstrates why sucrose and lactose are distinguished, i.e. due to their different diffusion coefficients. The diffusion coefficient values were taken from Ref. [33], however, a value was not found in the CRC for deoxyribose so it has been experimentally determined based on the calibration to be $0.85 \cdot 10^{-5} cm^2/s$. Thus, the sugar study further demonstrates the utility of the sensor as a means to measure diffusion coefficients in a microfluidic environment.

The μ-MMS was also evaluated as a universal detector for bench top HPLC applications. A size-exclusion chromatogram is shown in Fig. 7A from a mixture consisting of PEG 22 800 and PEG 106. The peak shape for the PEG 106 is narrow and uniform whereas the peak for PEG 22 800 is more broadened and also shows an additional peak at a higher molecular mass. These peak shape observations are consistent with the polydispersity values given in Table 1. PEG 106 is monodisperse and PEG 22 800 (polydispersity = 1.06) has some higher and lower molecular mass components. From the dual channel data in Fig. 7A one could also determine the concentration of the analytes via calibration using the signal collected at the upstream position. By taking the ratio of the downstream to upstream signals at the peak maximum, one can obtain diffusion coefficient and molecular mass information about the eluted peaks. These ratios were determined to be 0.916 for PEG 22 800 and 0.611 for PEG 106. The separation was repeated three times so the ratio values are averages and both had the same standard deviation of ±0.005, further demonstrating reproducibility.

The chromatographic data from Fig. 7A can also

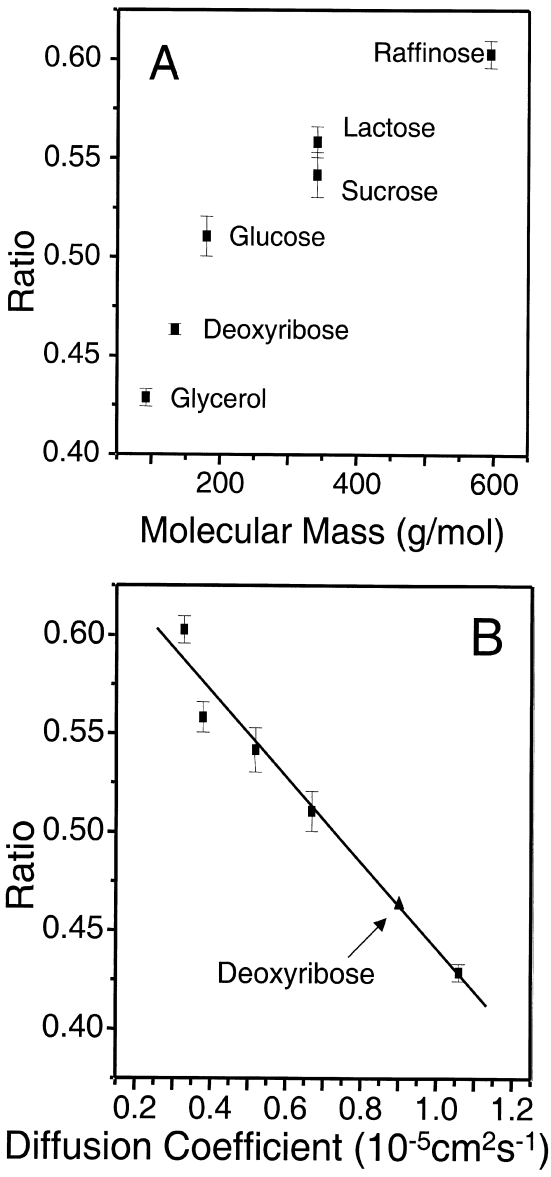

Fig. 6. (A) Ratio, *R*, as a function of molecular mass in g/mol for a series of sugars. Each point represents the average ratio taken from the downstream and upstream areas of three injections, and error bars are one standard deviation. A type A channel design was applied with a flow rate of 10 μl/min in the mobile phase stream and 5 μl/min sample stream where 20 μl of aqueous sugar solutions were injected at a concentration of 1‰. (B) Ratio as a function of diffusion coefficient. No diffusion coefficient was available in the CRC for deoxyribose. It was estimated as $0.85 \cdot 10^{-5}$ cm^2/s based on this calibration. The slope of the best-fit line for this small range of diffusion coefficients is −0.21, *y*-intercept is 0.66 with a correlation coefficient of 0.9902 for the linear regression.

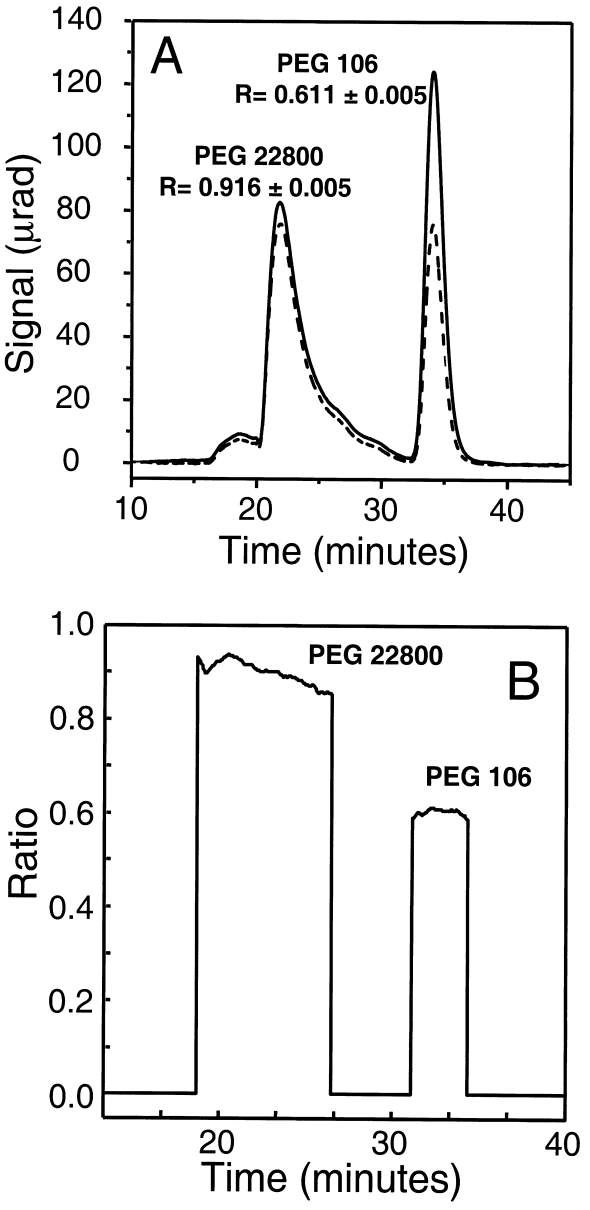

Fig. 7. (A) Size-exclusion chromatogram of a two-component mixture of PEG 22 800 and 106 collected with the μ-MMS. The dashed line represents the data collected at the downstream detection position while the solid line represents data collected at upstream detection position, corrected for the time delay of 5.3 s between two detection positions. The mixture has both PEGs at an injected concentration of 2‰, at 5 μl injected. A type B chip design was applied with a flow rate of 20 μl/min in both the mobile phase stream and the sample stream. (B) Ratiogram of the chromatograms in (A). A threshold of 9 μrad was applied for the ratiogram. For any part of the upstream-detected chromatogram with a signal less than 9 μrad, the ratio, *R*, was set to zero.

be presented as a ratiogram where the ratio of the downstream/upstream signal is plotted as a function of time as shown in Fig. 7B. The time-dependent ratiogram provides more information than is initially apparent from the chromatograms in Fig. 7A. Presenting the data as a ratiogram one can make predictions regarding the molecular mass, peak purity and polydispersity of an eluting analyte peak. This added information is complementary to the separation mechanism, be it SEC, reversed-phase HPLC, ion-exchange chromatography, etc. For example, by examining the degree of ''flatness'' of a given ratiogram peak, one can ascertain polydispersity for SEC. The PEG 106 is a monodisperse sample yielding a flat ratiogram response in Fig. 7B. Meanwhile, the more polydisperse PEG 22 800 exhibits a gradual downward sloping ratiogram. From SEC we know the broad peak tail for PEG 22 800 is due to the lower molecular mass components, which also agrees with the gradual downward slope of the ratio, consistent with the decreasing molecular mass of the eluting material. The additional peak just before the PEG 22 800 peak, eluting from 16 to 20 min, falls below the ratio threshold applied and is not present in the ratiogram. However, it had a ratio near that of the maximum for PEG 22 800, and is likely a higher molecular mass component. The ability of the μ-MMS to perform well for low molecular mass analytes indicates it is complementary to traditional light scattering detection for SEC, which is better suited to larger molecular mass analytes.

5. Conclusions

The μ-MMS provides useful and complementary information for FIA and HPLC applications, and should be a promising tool for a variety of μ-TAS applications. The new dual-beam instrument design has significantly improved the LOD and has made the sensor more useful by allowing for near real-time measurements. The sensor has also been used as a means for experimentally determining diffusion coefficients. This can be a very important application for CE as recently indicated [3], and especially for integration into CE and HPLC based μ-TAS. Continued research of this system will focus on targeting more specific applications where the μ-MMS can be most effective. This includes its use as a detector for LC, CE, and process monitoring. The chip will also be further developed to allow the sensor to be used for organic solvent-based systems.

6. Nomenclature

C	Analyte concentration
CE	Capillary electrophoresis
D	Analyte diffusion coefficient
DAQ	Data acquisition (Board)
FIA	Flow injection analysis
dC/dx	Distance-dependent analyte concentration gradient
dn/dC	Change in refractive index with concentration change
dn/dx	Distance-dependent analyte refractive index gradient
GRIN	Graded refractive index
HPLC	High performance liquid chromatography
L	Probe beam path length through microchip
LOD	Limit of detection
μ-MMS	Micromolecular mass sensor
μ-RIG	Microscale refractive index gradient
μ-TAS	Micro-total analysis system
MM	Molecular mass (average)
n_0	Solvent refractive index
PDMS	Poly(dimethyl siloxane)
PEG	Poly(ethylene glycol)
ppth	Parts per thousand, equivalent to ‰
PSD	Position sensitive detector
θ	Angle of deflection for probe beam (i.e. signal)
R	Ratio signal, downstream signal divided by upstream signal
RI	Refractive index
RIG	Refractive index gradient
SEC	Size-exclusion chromatography
x	Analyte migration distance due to diffusion

Acknowledgements

We thank the Center for Process Analytical

Chemistry (CPAC), a National Science Foundation initiated University/Industry Cooperative Research Center at the University of Washington for financial support.

References

[1] A. Manz, N. Graber, H.M. Widmer, Sensors Actuators B1 (1990) 244.
[2] J.P. Kutter, Trends Anal. Chem. 19 (2000) 352.
[3] C.T. Culbertson, S.C. Jacobson, J.M. Ramsey, Talanta 56 (2002) 365.
[4] C.D. Costin, R.E. Synovec, Talanta 58 (2002) 551.
[5] K. Swinney, D. Markov, D.J. Bornhop, Anal. Chem. 72 (2000) 2690.
[6] N. Burggraf, B. Krattiger, A.J. de Mello, N.F. de Rooij, A. Manz, Analyst 123 (1998) 1443.
[7] D. Markov, D. Begari, D.J. Bornhop, Anal. Chem. 74 (2002) 5438.
[8] C.D. Costin, R.E. Synovec, Anal. Chem. 74 (2002) 4558.
[9] D.J. Bornhop, N.J. Dovichi, Anal. Chem. 58 (1986) 504.
[10] D.J. Bornhop, N.J. Dovichi, Anal. Chem. 59 (1987) 1632.
[11] A.E. Bruno, B. Krattiger, F. Maystre, H.M. Widmer, Anal. Chem. 63 (1991) 2689.
[12] D.O. Hancock, C.N. Renn, R.E. Synovec, Anal. Chem. 62 (1990) 2441.
[13] L.R. Lima, R.E. Synovec, Anal. Chem. 65 (1993) 128.
[14] J. Pawliszyn, Anal. Chem. 58 (1986) 3207.
[15] J. Pawliszyn, M.F. Weber, M.J. Dignam, A. Mandelis, R.D. Venter, S. Park, Anal. Chem. 58 (1986) 236.
[16] J. Pawliszyn, Anal. Chem. 60 (1988) 2796.
[17] C.N. Renn, R.E. Synovec, J. Chromatogr. 536 (1991) 289.
[18] R.E. Synovec, Anal. Chem. 59 (1987) 2877.
[19] S.D. Woodruff, E.S. Yeung, Anal. Chem. 54 (1982) 1174.
[20] V. Murugaiah, R.E. Synovec, Anal. Chim. Acta 246 (1991) 241.
[21] V. Murugaiah, R.E. Synovec, Anal. Chem. 64 (1992) 2130.
[22] J.P. Brody, A.E. Kamholz, P. Yager, Proc. Micro. Nano-Fabric. Electro-Opt. Mech. Syst. Biomed. Environ. Appl. (1997) 103.
[23] R.F. Ismagilov, A.D. Stroock, P.J.A. Kenis, G. Whitesides, H.A. Stone, Appl. Phys. Lett. 76 (2000) 2376.
[24] A.E. Kamholz, B.H. Weigl, B.A. Finlayson, P. Yager, Anal. Chem. 71 (1999) 5340.
[25] A.E. Kamholz, P. Yager, Biophys. J. 80 (2001) 155.
[26] J.P. Brody, P. Yager, Sensors Actuators A 58 (1997) 13.
[27] P. Jandik, B.H. Weigl, N. Kessler, J. Cheng, C.J. Morris, T. Schulte, N. Avdalovic, J. Chromatogr. A 954 (2002) 33.
[28] C. Gaffney, C.K. Chau, Am. J. Phys. 69 (2001) 821.
[29] A.E. Kamholz, P. Yager, Sensors Actuators B 82 (2002) 117.
[30] Y. Xia, G.M. Whitesides, Angew. Chem., Int. Ed. 38 (1998) 550.
[31] D.C. Duffy, J.C. McDonald, O.J.A. Schueler, G.M. Whitesides, Anal. Chem. 70 (1998) 4974.
[32] P.G. Vahey, S.H. Park, B.J. Marquardt, Y. Xia, L.W. Burgess, R.E. Synovec, Talanta 51 (2000) 1205.
[33] D.R. Lide, CRC Handbook of Chemistry and Physics, CRC Press, Boca Raton, FL, 1995.